Journal of Neuroinflammation

RESEARCH

Open Access

Centripetal migration and prolonged retention of microglia promotes spinal cord injury repair

Jianan Ye[1†], Fangli Shan[1†], Xinzhong Xu[1,2†], Chao Liang[1†], Ningyuan Zhang[1], Hao Hu[1], Jianjian Li[1], Fangru Ouyang[1], Jingwen Wang[1], Yuanzhe Zhao[1], Zhida Ma[1], Congpeng Meng[1], Ziyu Li[1,2], Shuisheng Yu[1,2*], Juehua Jing[1,2*] and Meige Zheng[1,2*]

Abstract

Background Recent studies have confirmed the critical role of neonatal microglia in wound healing and axonal regeneration following spinal cord injury (SCI). However, the limited migration of microglia to the center of adult lesion may significantly impede their potential benefits.

Methods We established a model of microglial centripetal migration and prolonged retention in C57BL/6J and transgenic mice by injecting exogenous C-X3-C motif chemokine ligand 1 (CX3CL1) and macrophage colony-stimulating factor (M-CSF) directly into the lesion site post-SCI. Wound healing and axonal preservation/regrowth was assessed anatomically, and kinematics analysis was conducted to determine the recovery of locomotor function.

Results We identified decreased expression and perilesional distribution of CX3CL1 as the primary reason for the limited centripetal migration of microglia. In situ injection of CX3CL1 into the lesion core promoted microglial centripetal migration, but alone did not improve functional recovery. Nevertheless, a combinational administration of CX3CL1 and M-CSF fostered both centripetal migration and prolonged retention of microglia, thereby effectively displacing blood-derived macrophage infiltration and optimizing wound healing and axonal preservation/regrowth after SCI. Notably, the beneficial effects of CX3CL1 and M-CSF co-administration were specifically blocked in C-X3-C motif chemokine receptor 1 (CX3CR1)-deficient mice. These phenomena may be related to the increase in spleen tyrosine kinase (SYK) levels, which boosts centripetal microglial phagocytosis.

Conclusion Our study uncovers the criticality of microglial location and abundance in orchestrating SCI repair, highlighting centripetal microglial dynamics as valuable targets for therapeutic intervention.

†Jianan Ye, Fangli Shan, Xinzhong Xu and Chao Liang contributed equally to this work.

*Correspondence:
Shuisheng Yu
ysspaper@sina.com
Juehua Jing
jjhhu@sina.com
Meige Zheng
zhengmg113@126.com

Full list of author information is available at the end of the article

Keywords Spinal cord injury, Centripetal migration, Prolonged retention, CX3CL1, M-CSF

Introduction

The discovery of the scar-free repair function of neonatal microglia, as well as the loss- and gain-of-function experiments of adult microglia, have fully confirmed the indispensable role of microglia in spinal cord injury (SCI) repair [1–4]. Nevertheless, microglia-mediated tissue regeneration and repair in the microenvironment of adult SCI remains a great challenge. Notably, using the $LysM^{tdTom}$ > $Cx3Cr1^{GFP}$ chimera mouse model and lineage tracing strategies (e.g., $Cx3cr1^{creER}$::R26-TdT) have elucidated that C-X3-C motif chemokine receptor 1 (CX3CR1) tagged microglia predominantly localize at the border of lesion, while Mac-2 labeled blood-derived macrophages infiltrate into the lesion core [3, 5–7]. We suspect that such spatial segregation starkly limits the beneficial functions of microglia.

Microglial activation is largely regulated by the chemokine ligand CX3CL1 and its cognate receptor CX3CR1 [8]. CX3CL1, mainly synthesized by neurons and endothelial cells [9, 10], binds its sole receptor CX3CR1 on microglia, thereby orchestrating their recruitment to the site of neuroinflammation [11–13]. The CX3CL1/CX3CR1 axis is instrumental in microglial activation and migration, yet its influence on microglial distribution post-SCI has not been elucidated. Concurrently, several reports have consistently documented that the activation of colony-stimulating factor receptor (CSF1R) by macrophage colony-stimulating factor (M-CSF) plays a crucial role in ensuring the survival and repopulation of microglia [3, 14, 15]. Bellver-Landete1 et al. showed that an approximate 20–25% increase in microglial numbers via M-CSF hydrogel delivery at the SCI site limits tissue loss and improves locomotor recovery [3]. These suggest that promptly enhancing microglial presence and activity at the lesion core could be a promising SCI repair strategy.

In this study, we demonstrated that CX3CL1 is predominantly localized around the injury site and significantly reduced in the early stages of SCI. Remarkably, co-administration of CX3CL1 and M-CSF was proved to be a superior strategy to promote the centripetal migration and prolonged retention of microglia and effectively substitute for blood-derived macrophages, thereby optimizing wound healing and axonal preservation/regrowth compared to in situ injection of CX3CL1 or M-CSF alone after SCI. This synergistic effect appears to be associated with an increase in spleen tyrosine kinase (SYK) levels that enhance the phagocytic capacity of microglia after SCI.

Materials and methods

Animals and surgical procedures

The C57BL/6J (WT) female mice at age of 8 weeks were obtained from the Animal Experiment Center of Anhui Medical University. The $CX3CRl^{GFP}CCR2^{RFP}$ mice [16] and $CX3CR1^{-/-}$ ($CX3CR1^{GFP/GFP}$) mice [12] at age of 8 weeks were obtained from Jackson Laboratory (catalog no. 032127 and 005582). $CX3CR1^{+/-}$ ($CX3CR1^{+/GFP}$) mice were kindly donated by the Center for Excellence in Brain Science and Intelligence Technology, Chinese Acedamy of Sciences. All transgenic mice were bred to the C57BL/6J background. All mice were housed in a controlled environment with a 12-hour light-dark cycle, maintaining optimal humidity and temperature. The animals were randomly grouped and kept in specific pathogen-free (SPF) facility, where they were given unrestricted access to food and water. All procedures were carried out with the approval of the Ethics Committee of the Anhui Medical University (Approval No. LLSC20230809).

The spinal cord crush injury procedure was performed according to previously established methods [17]. The mice were anesthetized with isoflurane (induction 4%, maintenance 2%) before receiving midthoracic (T10) compression spinal cord injuries. The mice received a laminectomy at T7-8 vertebra to expose T10 spinal cord, and crush injury was performed with a calibrated Dumont #5 forceps (11252-20, Fine Science Tools, Germany) for 5 s. All SCI mice received Gentamycin (5 mg/kg, subcutaneous injection) and Buprenorphine (0.03 mg/kg, subcutaneous injection) to prevent infection and alleviate pain during the first week after surgery [18, 19]. Bladder care were performed twice daily throughout the study period.

In situ injection of CX3CL1 or M-CSF

The SCI mice was immobilized using the stereotaxic device, and the microinjection needle (7634-01 and 7803-05, Hamilton, Switzerland) was carefully inserted to a depth of 0.8 mm at the lesion epicenter [20]. One microliter of 100 ng/μl recombinant mouse CX3CL1 (458-MF-025, R&D Systems, USA) dissolved in sterile PBS (CX3CL1 group, $n = 10$) or 500 ng/μl recombinant mouse M-CSF (315-02, Proteintech, China) dissolved in sterile PBS (M-CSF group, $n = 8$) was injected into the epicenter of the injured spinal cord at 0.5 μl/min using a stereotaxic injector (KDS LEGATO 130, RWD, China) immediately after injury. Additionally, the injured mice in CX3CL1 + M-CSF group ($n = 24$) received the in situ injection of a 2 μl mixture containing 50 ng/μl recombinant mouse CX3CL1 and 250 ng/μl recombinant mouse

M-CSF. The control mice received 1 μl PBS (PBS group, $n = 10$) or heat-inactivated (95 °C for 45 min) CX3CL1 dissolved in sterile PBS (Control group, $n = 8$) [21]. After injection, the syringe was remained in the position for one minute before being carefully withdrawn. Finally, the mice were sacrificed at either 7 or 28 days after injection.

Tissue preparation and immunofluorescent staining

Mice were perfused with ice-cold 0.1 M PBS (Servicebio, China), followed by 4% paraformaldehyde (PFA, Servicebio, China). An 8 mm mouse spinal cord segment centered at the injury site was placed in 4% PFA and post fixed for 5 h. The tissue was then placed in 30% sucrose solution and dehydrated at 4 °C for 24–48 h. Finally, it was embedded in OCT (Biosharp, China), and sagittal sections were cut serially at 16 μm using a cryostat (NX50, Thermo Fisher Scientific, USA). The sections were baked at 50 °C for 1 h and blocked using a solution of 10% normal donkey serum in PBS containing 0.3% Triton X-100 (SL050 and T8200, Solarbio, China) at room temperature for 1 h. The primary antibodies were incubated at 4 °C overnight. The primary antibodies included rabbit anti-CX3CL1 (1:100, ab25088, Abcam, USA), goat anti-CX3CL1 (1:50, AF537, R&D Systems, USA), goat anti-Iba-1(1:200, NB100-1028, Novus Biologicals, USA), goat anti-CD31 (1:200, AF3628, R&D Systems, USA), chicken anti-GFP (1:500, GFP1010, Aves Labs, USA), rabbit anti-Fascin-1 (1:100, ab126772, Abcam, USA), rat anti-Mac-2 (1:100, sc23938, Santa Cruz Biotechnology, USA), rat anti-GFAP (1:400, 13–0300, Thermo Fisher Scientific, USA), goat anti-PDGFRβ (1:100, AF1042-SP, R&D Systems, USA), rabbit anti-NeuN (1:500, ab177487, Abcam, USA), goat anti-5-hydroxytryptamine (5-HT) (1:500, 20079, Immunostar, USA), chicken anti-RFP (1:500, 600-901-379, Rockland, USA), rabbit anti-SYK (1:100, 13198, Cell Signaling Technology, USA), rat anti-Ki67 (1:100, 14-5698-80, Invitrogen, USA). Subsequently, the appropriate secondary antibodies were incubated for 1 h at room temperature, including donkey anti-goat Alexa Fluor 488, donkey anti-rabbit Alexa Fluor 555, donkey anti-rat Alexa Fluor 488, donkey anti-rat Alexa Fluor 555 and donkey anti-goat Alexa Fluor 555, donkey anti-rabbit Alexa Fluor 488 (1:500, A-11055, A-31572, A-21208, A-48270, A-21432, A-21206, Thermo Fisher Scientific, USA); donkey anti-chicken Alexa Fluor 488 and donkey anti-chicken Alexa Fluor 594 (1:500, 703-545-155, 703-585-155, Jackson Immuno Research Laboratories Inc, USA). Finally, DAPI (C1005, Beyotime Biotechnology, China) staining was used to label cell nuclei. The negative control sections incubated with secondary antibody alone were all showed no staining.

ORO staining

Oil red O (ORO) staining was performed using a modified ORO Staining Kit (C0158S, Beyotime Biotech, China). Briefly, frozen sections were washed with PBS and then incubated in 60% isopropanol for 20–30 s. The modified ORO staining solution was added to the sections and incubated for 10–15 min at room temperature. Following staining, tissue sections were thoroughly rinsed with 60% isopropanol until complete removal of residual dye was achieved, as confirmed by the absence of visible staining in non-lesioned areas under macroscopic examination. Finally, the sections were mounted with glycerol and observed under a microscope (Zeiss Axio Scope A1, Zeiss, Germany).

TUNEL assay

The frozen sections were prepared for the terminal deoxynucleotidyl transferase dUTP nick-end labeling (TUNEL) staining using a TUNEL Apoptosis Assay Kit (12156792910, Roche, Switzerland). According to the manufacturer's instructions, the sections were incubated at 50 °C for 1 h and then washed with PBS. The sections were permeabilized with 0.1% Triton X-100 in 0.1% sodium citrate for 2 min at 2–8 °C. After washing with PBS, the sections were incubated with freshly prepared TUNEL reaction mixture in a dark and humid environment for 1 h at 37 °C. The DAPI staining was used to label cell nuclei. Finally, the sections were observed under a microscope (Zeiss Axio Scope A1, Zeiss, Germany) to visualize the results of the staining.

Image acquisition and quantitative analysis

Representative images were acquired using a Zeiss Axio Scope A1 fluorescence microscope and a Pannoramic MIDI section Digital Scanner. ImageJ software (version for Windows 64-bit, NIH, USA) was used for image processing.

To quantify Fascin-1$^+$ and GFP$^+$ microglia, Fascin-1$^+$ and GFP$^+$ cells were counted in 40 × images of the epicenter. The data of each sample was determined by averaging three randomly selected images at a magnification of 40 ×, with 3 samples per group.

To evaluate neuron preservation, the spinal cord segments located at various distances up to 1 mm adjacent to the lesion borders were segmented into Z1, Z2, and Z3 zones of 250 μm width in a 5 × image, and NeuN$^+$ cells were counted in each zone [22, 23]. To determine the proportional area of tissue occupied by fibrotic scar, the PDGFRβ$^+$ area was normalized to the area of the spinal cord segment spanning the injured core in a 5 × image [5]. Similarly, the GFAP$^-$ area, Mac-2$^+$ area, RFP$^+$ area, and SYK$^+$ area was normalized to the area of the spinal cord segment spanning the injured core in a 5 × image. In addition, the fluorescence density was used for

quantifying the expression of CX3CL1, 5-HT, and ORO. Exposure time and gain were kept constant between conditions for each fluorescence channel. For each sample, the spinal cord sections spanning the injured core and two adjacent spinal cord sections spaced 100 μm apart were quantified. The date from each section were averaged, with 3–5 samples per group.

All quantifications were done blindly with respect to the identity of the animals.

Behavioral analysis

The locomotor recovery of the mice was evaluated in a blinded manner by two experienced examiners using the Basso Mouse Scale (BMS) score prior to injury and at various time points (0, 3, 7, 14, 21, and 28 days) after SCI [24]. The average of the scores of both hind limbs obtained from two investigators was used as the final data.

The footprint analysis was performed to further evaluate kinematics at 4 weeks after SCI, as previously described [24]. Green and red dyes were painted on the front and hind paws of the mice, respectively. Subsequently, the mice were allowed to walk on a narrow track (long 80 cm and width 4 cm). The stride length was determined by the distance between the hind paws of the previous step and the following step. The distance of the outermost toe of the left paw to the outermost toe of the right paw was used to determine stride width. Paw rotation was determined by the angle between the midline axis of the hind paw and the midline axis of the body. For all evaluations, three consecutive gait cycles were measured in the bilateral hind paws, and the average value was taken as the final data for each mouse.

Statistical analysis

The data were shown as individual data points, with error bars representing the mean ± standard error of the mean (SEM). The GraphPad Prism 6.0 (GraphPad, USA) was used for data analysis. For comparison between the two groups, Student's unpaired t-tests was used. For multiple comparisons, one-way or two-way analysis of variance (ANOVA) followed by Bonferroni post hoc tests was used. A p value < 0.05 was statistically significant.

Results

Neuron and endothelial cell-derived CX3CL1 is distributed around the SCI lesion site

Microglia, following SCI, are known to aggregate at the border of the lesion, forming neuroprotective structures referred to as "microglial scars" [3]. However, the specific mechanism governing microglial distribution and its potential correlation with the expression of the chemokine CX3CL1 remain to be elucidated. To address this gap, we conducted immunofluorescence staining for Iba-1 and CX3CL1 pre-SCI and at 3, 7, 14, 28 days post-injury (dpi). The results showed that both CX3CL1 and microglia were predominantly localized at the edge of lesion core, suggesting a spatially and temporally coordinated interaction between the two (Fig. 1A, B). Notably, CX3CL1 expression was significantly reduced at 3 and 7 dpi, before returning to baseline levels between 14 and 28 dpi ($n = 5$ mice per group/time point, $^{*}P < 0.05$, $^{**}P < 0.01$, $^{***}P < 0.001$ and $^{****}P < 0.0001$, Fig. 1B, C). Further, we identified the cellular sources of CX3CL1 using antibodies against NeuN (a neuronal marker) and CD31 (an endothelial cell marker), revealing co-localization of CX3CL1 with both NeuN and CD31 in the lesion penumbra (Fig. S1A, B). This suggests that neurons and endothelial cells are the primary sources of CX3CL1 in the injured spinal cord.

In addition, utilizing $CX3CR1^{+/-}$ ($CX3CR1^{+/GFP}$) or $CX3CR1^{-/-}$ ($CX3CR1^{GFP/GFP}$) transgenic mice, where microglia are GFP-labelled, we further confirmed the primary localization of microglia and CX3CL1 at the edge of the lesion core at 14 dpi (Fig. S1C, D). However, in these CX3CR1-deficient mice, the distribution of CX3CL1 and GFP-labelled microglia was notably dispersed and misaligned (Fig. S1D), contrasting with the mutual contact or co-staining observed in wild-type (WT) SCI mice (Fig. 1B). This indicates that CX3CL1 functions as a chemoattractant for microglial migration, necessitating the presence of the receptor CX3CR1. Overall, our data underscore the impact of diminished CX3CL1 levels and its perilesional distribution on the localization and function of microglia after SCI.

In situ injection of CX3CL1 promotes centripetal migration of microglia after SCI

Given the localization of CX3CL1 and microglia at the lesion periphery post-SCI, we sought to investigate whether microglia could migrate towards the lesion epicenter in response to CX3CL1. We administered recombinant mouse CX3CL1 (CX3CL1 group) via in situ injection immediately after SCI in mice, alongside control injections of heat-inactivated CX3CL1 (Control group) and PBS (PBS group) (Fig. 1D). Immunohistochemical analysis of injured spinal cords revealed elevated CX3CL1 levels at the lesion site in the CX3CL1 group compared to the Control and PBS groups at 7 dpi ($n = 3$ mice per group, $^{****}P < 0.0001$, Fig. 1E, H). We utilized Fascin-1 as a specific microglial marker, given its specific expression in $CX3CR1^{+}$ microglia at the lesion edge, while not being expressed in macrophages within the lesion core, as reported in our previous study [25]. We observed a significantly higher number of Fascin-1^{+} microglia within the lesion core at 7 dpi in the CX3CL1 group compared to the Control and PBS groups ($n = 4$ mice per group, $^{****}P < 0.0001$, Fig. 1F, I), suggestive

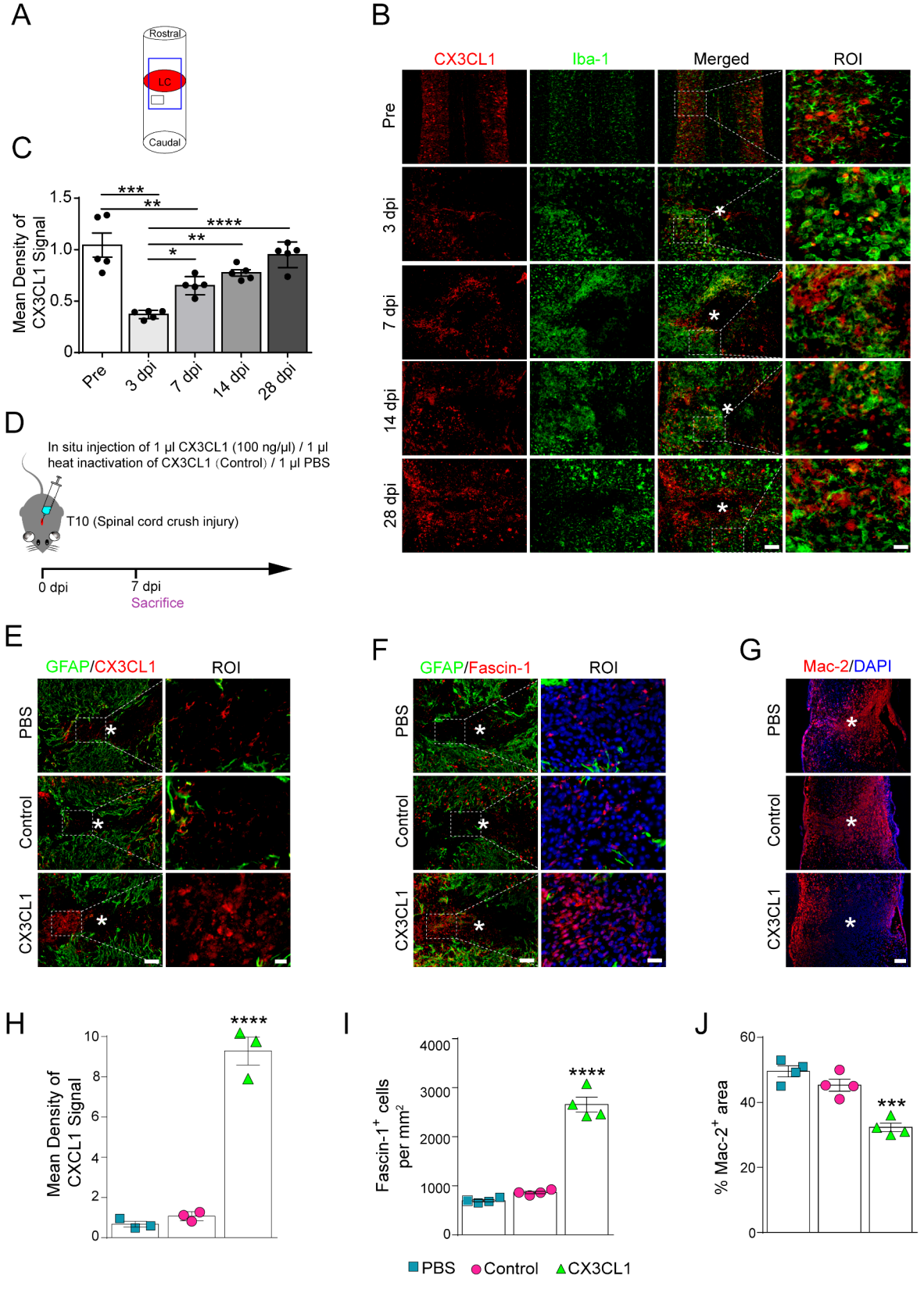

Fig. 1 (See legend on next page.)

(See figure on previous page.)

Fig. 1 In situ injection of CX3CL1 into the injured spinal cord enhances microglial migration towards the epicenter. **(A)** Schematic illustration of the experimental design depicts the lesion core (LC), with the large blue rectangle delineating the low-magnification field of view and the inset box indicating the corresponding region for high-magnification imaging presented in panel B. **(B)** Representative images of immunofluorescent staining of spinal cord with Iba-1 (green) and CX3CL1 (red) in sagittal sections before SCI (Pre) and at 3, 7, 14 and 28 dpi. The region of interest (ROI) represents the high-magnification image within the dotted box on the left. Asterisks show the injured core. **(C)** Quantification of the mean density of CX3CL1 signals at different time points within the lesion site ($n=5$ mice per group/time point). **(D)** Schematic diagram illustrating in situ injection of 1 μl CX3CL1 (CX3CL1group), heat inactivation of CX3CL1 (Control group) or PBS (PBS group) into the epicenter immediately after SCI. Immunofluorescent staining was performed at 7 dpi. **(E)** GFAP (green) and CX3CL1 (red) staining of the injured cords from the CX3CL1, Control, and PBS groups at 7 dpi. **(F)** Immunofluorescence staining of GFAP (green) and Fascin-1 (red) reveals the centripetal migration of Fascin-1$^+$ microglia at the injury sites in the CX3CL1 group compared to the control and PBS groups at 7 dpi. **(G)** Immunofluorescence staining of Mac-2 (red) and DAPI (blue) in sagittal sections from the CX3CL1, Control and PBS groups at 7dpi. **(H)** Quantification of the density of CX3CL1$^+$ signal in the epicenter at 7 dpi ($n=3$ mice per group). **(I and J)** Quantification of the number of Fascin-1$^+$ cells (**I**) in the epicenter and percentage of Mac-2$^+$ area (J) within the spinal cord segment spanning the injured core at 7 dpi ($n=4$ mice per group). The data are presented as means ± SEM (error bars). $^{*}P<0.05$ and $^{**}P<0.01$, $^{***}P<0.001$ and $^{****}P<0.0001$. Statistical analysis was performed using one-way ANOVA followed by Bonferroni post hoc tests. Scale bars = 100 μm (**B**, **E** and **F**), 200 μm (**G**), 20 μm (**ROI**)

of centripetal migration of microglia in response to CX3CL1 in situ injection. Concurrently, the extent of Mac-2$^+$ macrophage infiltration was significantly reduced in the CX3CL1-injected mice post-SCI, compared to controls ($n=4$ mice per group, $^{***}P<0.001$, Fig. 1G, J). These findings indicate that CX3CL1-induced successful centripetal migration of microglia can supplant blood-derived macrophage infiltration after SCI.

Microglial centripetal migration alone does not significantly influence scar formation and neuron preservation after SCI

Next, we examined the impact of microglial centripetal migration on scar formation and neuron preservation following SCI. Immunofluorescence staining results revealed no discernible difference in GFAP$^-$ lesion area or PDGFRβ$^+$ fibrotic scar formation among the CX3CL1, Control, and PBS groups at 28 dpi ($n=4$ mice per group, $P>0.05$, Fig. 2A-C). Furthermore, NeuN staining in specific zones (Z1-Z3) located at varying distances from the lesion core showed no significant impact of microglial migration on the number of preserved neurons in the CX3CL1 group compared to the Control and PBS groups at 28 dpi ($n=3$ mice per group, $P>0.05$, Fig. 2D, E). In conclusion, these results suggest that microglial centripetal migration alone has no significant effect on scar formation and neuron preservation after SCI.

Co-administration of CX3CL1 and M-CSF enhances both centripetal migration and prolonged retention of microglia after SCI

The functional dynamics of microglia post-SCI may be intricately linked to their population density. Previous studies have shown that administration of M-CSF can stimulate microglial proliferation during critical periods, thereby limiting tissue loss and enhancing functional recovery [3]. To explore the potential relationship between microglial function and their quantity, we co-administered CX3CL1 and M-CSF (CX3CL1 + M-CSF group) to boost both microglial migration and proliferation in vivo (Fig. 3A). As a control, in situ injection of recombinant mouse M-CSF (M-CSF group) were also performed. Immunofluorescence staining showed that there were significantly more Fascin-1$^+$ microglia in the epicenter of the CX3CL1 + M-CSF group compared with the CX3CL1 group and M-CSF group at 28 dpi ($n=4$ mice per group, $^{****}P<0.0001$, Fig. 3B, C). Interestingly, the number of Fascin-1$^+$ cells in the CX3CL1 group exhibited a significant decline within the lesion core at 28 dpi relative to 7 dpi (Fig. 1F, I; Fig. 3B, C). To assess the impact of in situ injection of CX3CL1 + M-CSF, CX3CL1, and M-CSF on microglial migration and retention within the injury core, we detected the proliferation and apoptosis of microglia using Fascin-1, Ki67, and TUNEL staining at 7 and 28 dpi. Our findings unveiled a robust enhancement in Ki67$^+$ cell proliferation in the CX3CL1 + M-CSF and M-CSF groups compared to the CX3CL1 group at 7 dpi (Fig. 4A, C). Additionally, the CX3CL1 group showed noticeable TUNEL$^+$ cell apoptosis relative to the CX3CL1 + M-CSF and M-CSF groups at 28 dpi (Fig. 4B, D). These observations shed light on the reason of the diminished presence of migrating microglia within the injury core in the CX3CL1 group at 28 dpi. Importantly, Fascin-1 staining revealed pronounced centripetal migration of microglia in the CX3CL1 + M-CSF group at both 7 and 28 dpi. In stark contrast, the injured core of the M-CSF group displayed a paucity of Fascin1$^+$ cells (Fig. 4), indicating M-CSF's limited capacity to promote microglial migration. Moreover, the observed increase in Ki67$^+$ proliferating cells at 7 dpi in the M-CSF group (Fig. 4A) suggests that these cells may be macrophages rather than microglia (Fig. 3D, E). Our findings collectively demonstrate that co-administration of CX3CL1 and M-CSF promotes both centripetal migration and prolonged retention of microglia, surpassing the effects of administering CX3CL1 or M-CSF alone post-SCI.

Further analysis revealed a relative reduction of Mac-2$^+$ macrophages in the CX3CL1 + M-CSF group compared to the CX3CL1 and M-CSF groups after SCI ($n=4$ mice per group, $^{****}P<0.0001$, Fig. 3D, E). This observation was further validated in the CX3CR1^{GFP}CCR2^{RFP} transgenic

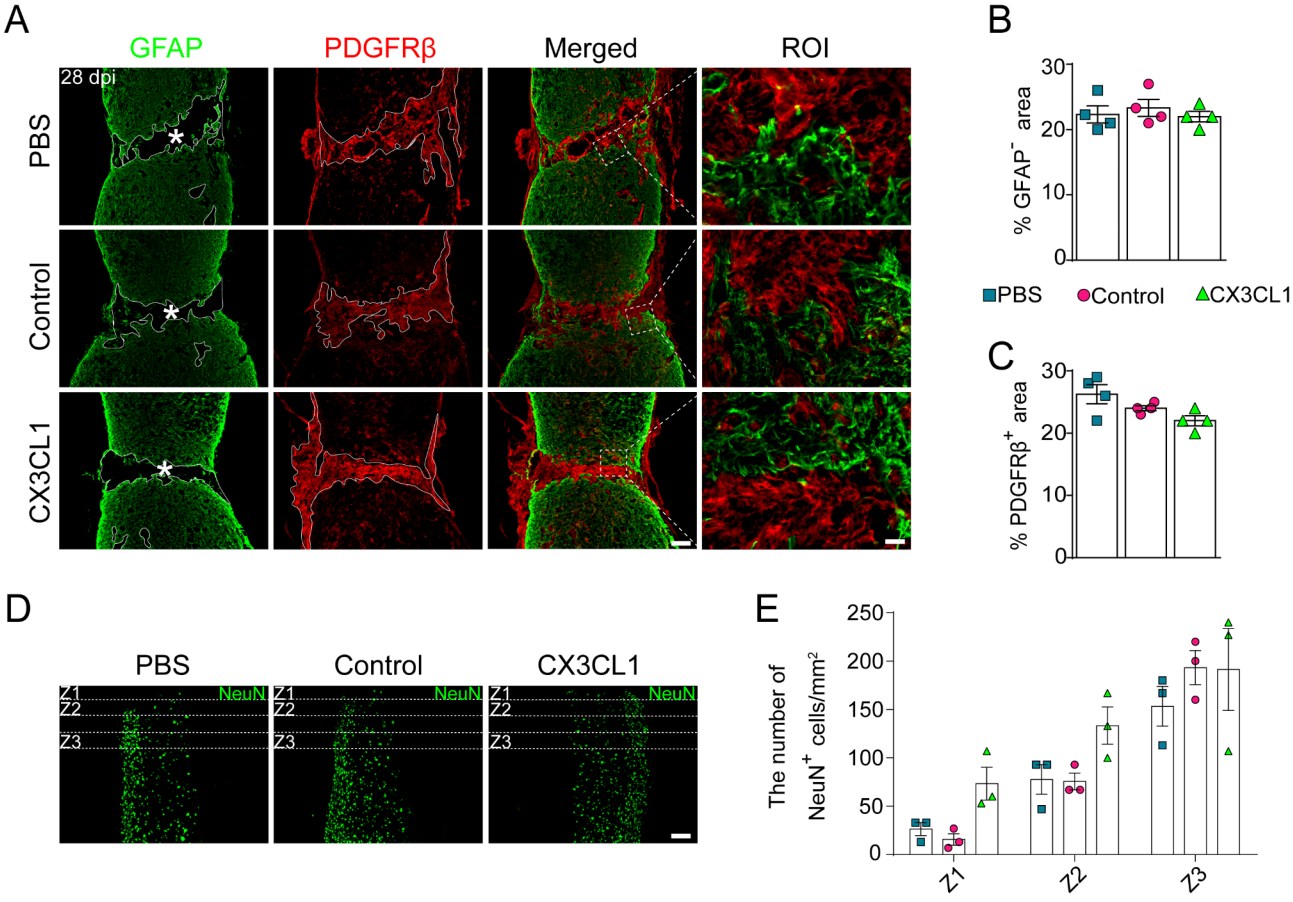

Fig. 2 The early centripetal migration of microglia alone does not significantly contribute to scar formation and neuron preservation after SCI. (**A**) Immunofluorescence staining of GFAP (green) and PDGFRβ (red) in sagittal sections from the CX3CL1, Control and PBS groups at 28 dpi. ROI represents the high-magnification image within the dotted box on the left. Asterisks show the injured core. (**B** and **C**) Quantification of the percentage of GFAP− area (**B**) and PDGFRβ+ area (**C**) within the spinal cord segment spanning the injured core at 28 dpi ($n = 4$ mice per group). (**D**) Representative immunofluorescence images of NeuN+ neurons in Z1–Z3 zones adjacent to central lesion core in the CX3CL1, Control and PBS groups at 28 dpi. (**E**) Quantification of NeuN+ neurons in Z1–Z3 zones adjacent to central lesion core in the CX3CL1, Control and PBS groups at 28 dpi ($n = 3$ mice per group). The data are presented as means ± SEM (error bars). Statistical analysis was performed using either one-way (**B** and **C**) or two-way (**E**) ANOVA followed by Bonferroni post hoc tests. Scale bars = 200 μm (A and D), 20 μm (**ROI**)

mouse model, where the percentage of RFP^+ macrophages in the injury epicenter was significantly lower in the CX3CL1 + M-CSF injection group compared to the PBS injection group at 28 dpi ($n = 3$ mice per group, $^{****}P < 0.0001$, Fig. 3F, G). Altogether, our results confirm the cooperative role of M-CSF and CX3CL1 in mediating centripetal migration and prolonged retention of microglia while effectively mitigating macrophage infiltration following SCI.

Centripetal migration and prolonged retention of microglia promotes wound healing, axonal preservation/regrowth and locomotor functional recovery after SCI

The potential therapeutic effects of co-administration of CX3CL1 and M-CSF on SCI recovery were further explored. Immunofluorescence staining analysis revealed that the CX3CL1 + M-CSF group showed a significant reduction in $GFAP^-$ lesion area and $PDGFR\beta^+$ fibrotic scar formation and an increase in the number of neurons within Z1–Z3 zones ($n = 3$ or 4 mice per group, $^{*}P < 0.05$, $^{**}P < 0.01$, $^{***}P < 0.001$ and $^{****}P < 0.0001$, Fig. 5), along with elevated 5-HT^+ fiber density and enhanced 5-HT^+ axonal preservation/regrowth across the lesion site at 28 dpi compared with the PBS group ($n = 3$ mice per group, $^{***}P < 0.001$, Fig. 6A, B). Conversely, no significant differences were observed between the CX3CL1 group, the M-CSF group, the PBS group, and the Control group (Fig. 5; Fig. 6A, B).

Concurrently, mice in the CX3CL1 + M-CSF combination treatment group demonstrated remarkable motor function recovery, as evidenced by higher BMS scores and improved hind limb locomotor performance at 14, 21 or 28 dpi compared to the PBS and the monotreatment groups ($n = 8$ mice per group, $^{*}P < 0.05$, $^{**}P < 0.01$, $^{***}P < 0.001$, $^{****}P < 0.0001$, Fig. 6C-G). In contrast, no obvious disparities in BMS score or foot print analysis were

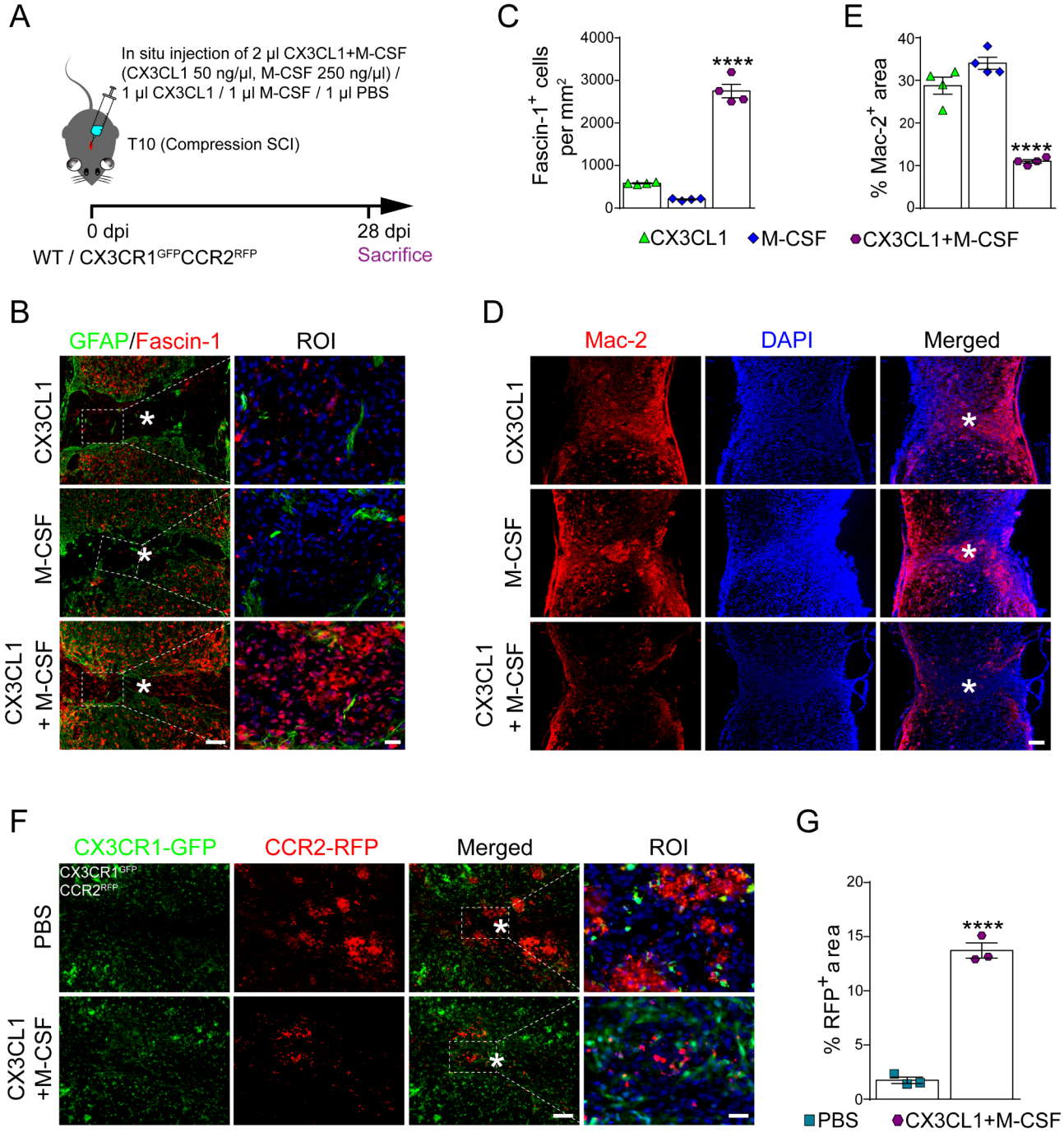

Fig. 3 Co-administration of CX3CL1 and M-CSF enhances centripetal migration and prolonged retention of microglia after SCI. (**A**) Schematic diagram illustrating in situ injection of 2 µl CX3CL1 and M-CSF (CX3CL1 + M-CSF group), 1 µl CX3CL1 (CX3CL1 group), 1 µl M-CSF (M-CSF group) or 1 µl PBS (PBS group) into the epicenter immediately after SCI in WT and $CX3CR1^{GFP}CCR2^{RFP}$ mice. Histological analysis was performed at 28 dpi. (**B**) Immunofluorescence staining of GFAP (green) and Fascin-1 (red) showing an augmented presence of Fascin-1^+ microglia at the injury sites in the CX3CL1 + M-CSF group compared to the CX3CL1 and M-CSF groups at 28 dpi of WT mice. ROI represents the high-magnification image within the dotted box on the left. Asterisks show the injured core. (**C**) Quantification of the number of Fascin-1^+ cells in the epicenter at 28 dpi ($n = 4$ mice per group). (**D**) Immunofluorescence staining of Mac-2 (red) and DAPI (blue) in sagittal sections from the CX3CL1 + M-CSF, CX3CL1 and M-CSF groups at 28 dpi of WT mice. (**E**) Quantification of the percentage of Mac-2^+ area within the spinal cord segment spanning the injured core at 28 dpi ($n = 4$ mice per group). (**F**) Representative immunofluorescence images of RFP (red) and GFP (green) in sagittal sections of the injured spinal cord from the CX3CL1 + M-CSF and PBS groups at 28 dpi of $CX3CR1^{GFP}CCR2^{RFP}$ mice. (**G**) Quantification of the percentage of RFP^+ area within the spinal cord segment spanning the injured core at 28 dpi ($n = 3$ mice per group). The data are presented as means ± SEM (error bars). $^{****}P < 0.0001$, the CX3CL1 + M-CSF group versus the CX3CL1, M-CSF and PBS groups. Statistical analysis was performed using one-way ANOVA followed by Bonferroni post hoc tests (**C** and **E**), or Student's two-tailed unpaired t-test (**G**). Scale bars = 100 µm (**B** and **F**), 200 µm (**D**), 20 µm (**ROI**)

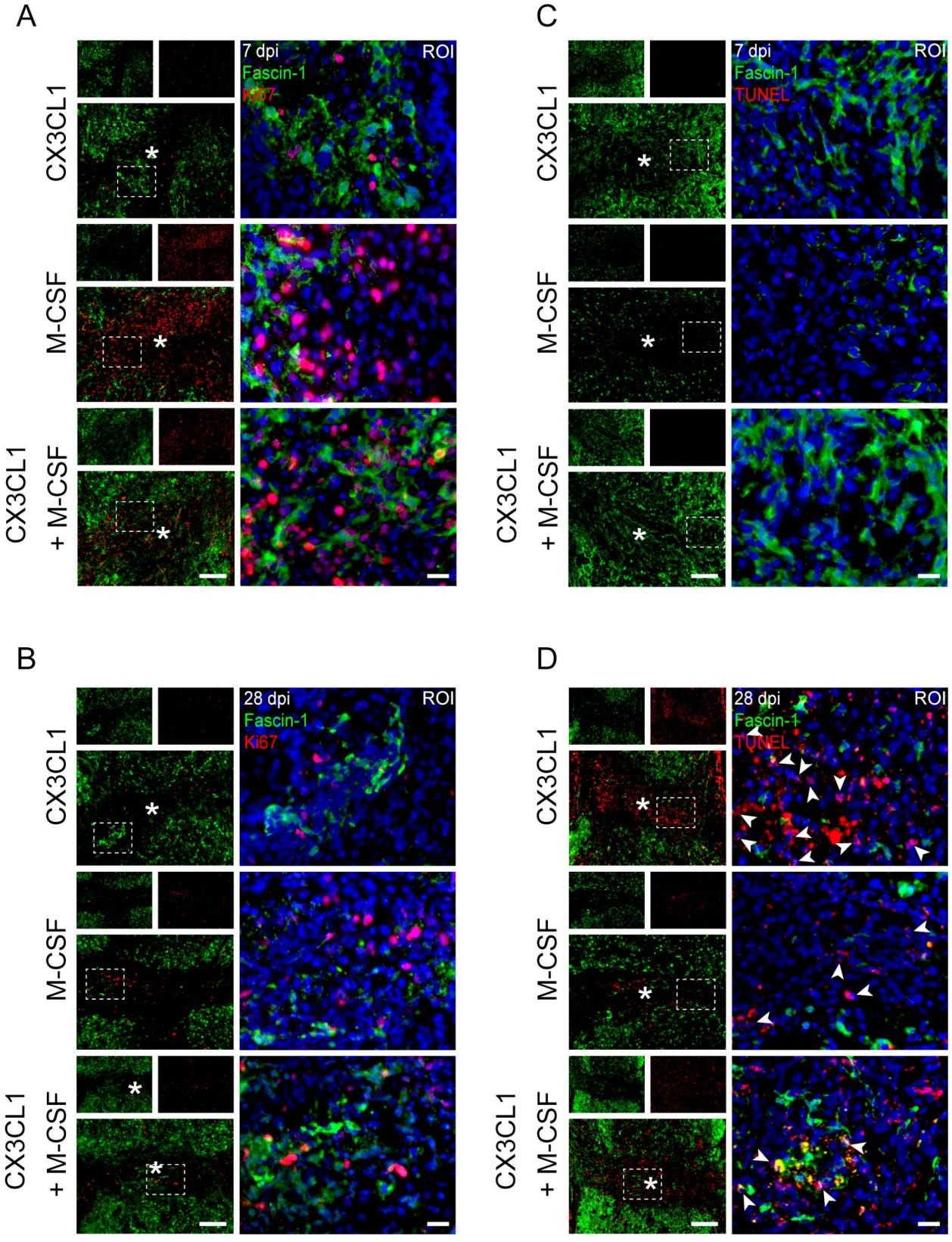

Fig. 4 (See legend on next page.)

(See figure on previous page.)

Fig. 4 Microglial proliferation and apoptosis in the epicenter at 7 and 28 dpi after in situ injection. **(A and B)** Images of spinal cord sections from the CX3CL1 + M-CSF, CX3CL1, and M-CSF groups stained with antibodies against Fascin-1 and Ki67 at 7 dpi or 28 dpi. **(C and D)** Images of spinal cord sections from the CX3CL1 + M-CSF, CX3CL1, and M-CSF groups stained with antibodies against Fascin-1 and TUNEL at 7 dpi or 28 dpi. White arrowheads indicate the apoptosis of cell (D). ROI represents the high-magnification image within the dotted box on the left. Asterisks show the injured core. Scale bars = 100 μm, 20 μm (**ROI**).

noted between the other groups ($n = 8$ mice per group, $P > 0.05$, Fig. 6C-G). Altogether, these data indicate the significance of centripetal migration and prolonged retention of microglia in promoting optimal functional recovery after SCI.

The beneficial effects of combined administration of CX3CL1 and M-CSF are specifically blocked in CX3CR1$^{-/-}$ mice

To further confirm that the combined injection of CX3CL1 and M-CSF works through specifically targeting the receptor CX3CR1 on microglia, we conducted the co-administration experiments on both CX3CR1$^{+/-}$ and CX3CR1$^{-/-}$ mice immediately post-SCI (Fig. 7A). Consistent with prior observations in WT mice (Fig. 3B, C), the co-administration also significantly augmented the distribution of GFP-labelled microglia within the injury core in CX3CR1$^{+/-}$ mice ($n = 3$ mice per group, $^{****}P < 0.0001$, Fig. 7B, C). However, in CX3CR1$^{-/-}$ mice, characterized by the absence of the CX3CR1 receptor, this treatment proved ineffective in promoting centripetal migration of microglia (Fig. 7B, C).

Meanwhile, the GFAP^{-} lesion area and PDGFRβ^{+} fibrotic scar formation were markedly elevated, and the retention of NeuN^{+} neurons within the Z1–Z3 zones was significantly reduced in CX3CR1$^{-/-}$ mice compared to their CX3CR1$^{+/-}$ counterparts at 28 dpi ($n = 3$ mice per group, $^{*}P < 0.05$ and $^{**}P < 0.01$, Fig. 7D-G). Furthermore, 5-HT^{+} fiber density exhibited a pronounced decrease, and there was a notable absence of axonal preservation/regrowth across the lesion site in CX3CR1$^{-/-}$ mice contrast to CX3CR1$^{+/-}$ mice ($n = 3$ mice per group, $^{**}P < 0.01$, Fig. 7H, I). These deficits were accompanied by inferior motor recovery in CX3CR1$^{-/-}$ mice, as evidenced by lower BMS scores and compromised foot print analysis at 14, 21 and 28 dpi, compared to CX3CR1$^{+/-}$ mice ($n = 6$ mice per group, $^{*}P < 0.05$, $^{***}P < 0.001$ and $^{****}P < 0.0001$, Fig. 7J-L). Collectively, these data unequivocally substantiate that the beneficial effects of CX3CL1 and M-CSF co-administration are specifically blocked in CX3CR1$^{-/-}$ mice when compared to their CX3CR1$^{+/-}$ counterparts, emphasizing the pivotal role of the CX3CR1 receptor in mediating these therapeutic outcomes.

Centripetal migration and prolonged retention of microglia mitigates the accumulation of foamy macrophages by increasing SYK levels after SCI

Recent studies have elucidated that the spleen tyrosine kinase (SYK) signaling plays a critical role in reprogramming microglia towards a disease-associated phenotype with enhanced tropism and efficient phagocytic clearance ability for pathological amyloid beta deposits in Alzheimer's disease models [26, 27]. To investigate the potential contribution of SYK signaling to the observed benefits of centripetal migration and prolonged retention of microglia post-SCI, we performed immunofluorescence staining of SYK in all groups. Our analysis revealed a significant elevation in SYK levels at the lesion site in the CX3CL1 + M-CSF group compared to the M-CSF, Control and PBS groups at 28 dpi ($n = 4$ mice per group, $^{**}P < 0.01$, $^{***}P < 0.001$ and $^{****}P < 0.0001$, Fig. 8A, B). Consistently, Oil Red O (ORO) staining unveiled a notable reduction in foamy macrophages within the lesion core of the CX3CL1 + M-CSF group relative to the other groups at 28 dpi ($n = 3$ mice per group, $^{*}P < 0.05$, Fig. 8C, D), aligning with the increased SYK expression. No significant differences were found in SYK expression levels or foamy macrophage accumulation between the CX3CL1 group, the M-CSF group, and the Control or PBS groups at 28 dpi ($n = 3$ or 4 mice per group, $P > 0.05$, Fig. 8A-D). Moreover, the expression level of SYK in CX3CR1$^{+/-}$ mice displayed a significant augmentation compared to CX3CR1$^{-/-}$ mice at 28 dpi following the co-administration of CX3CL1 and M-CSF ($n = 3$ mice per group, $^{**}P < 0.01$, Fig. 8E, F). Taken together, our data suggest that the beneficial effects of the co-administration of CX3CL1 and M-CSF appear to be associated with elevated SYK levels, which potentially enhance the phagocytic efficiency of the centripetal microglia after SCI.

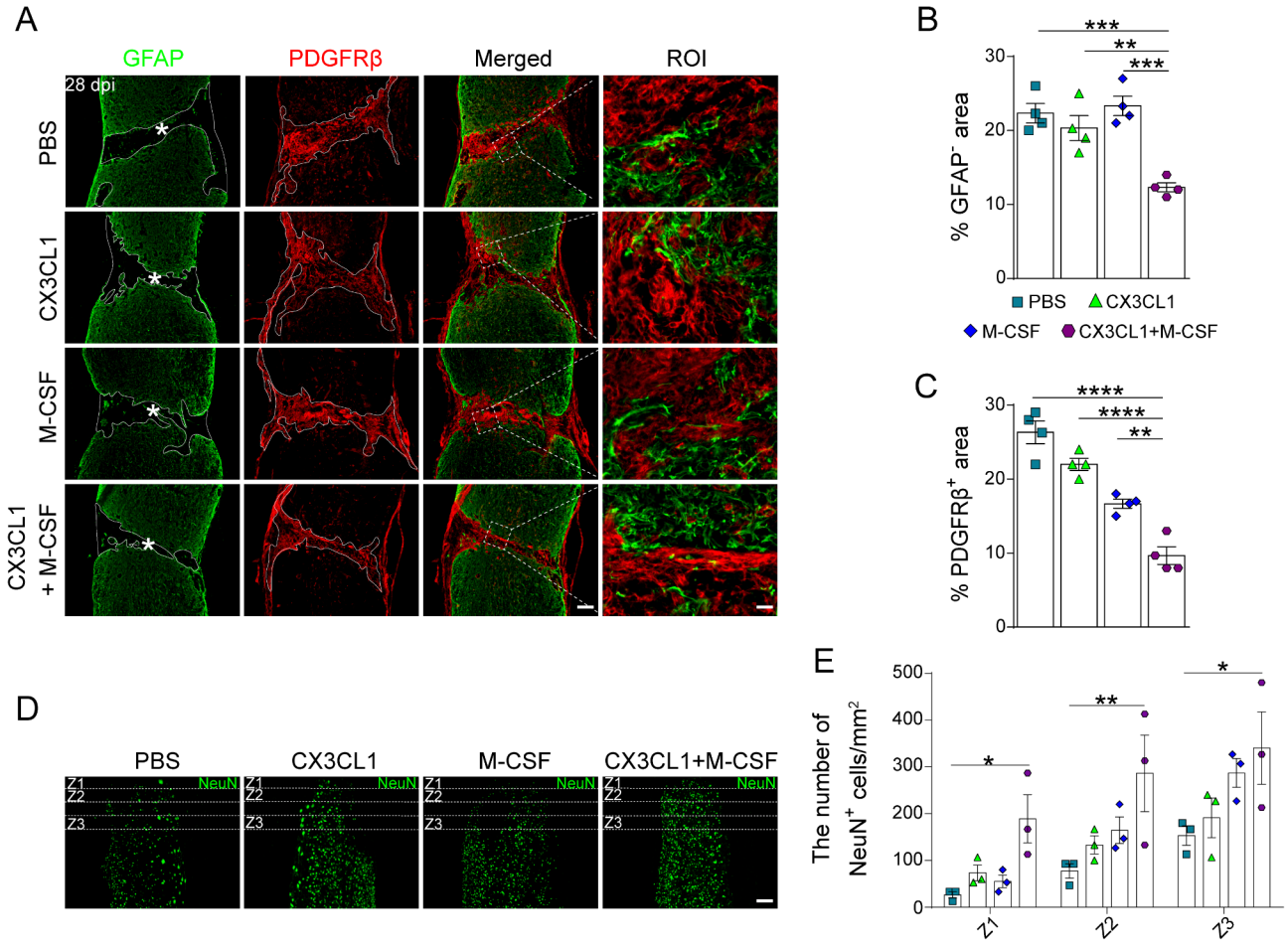

Fig. 5 Co-administration of CX3CL1 and M-CSF effectively diminishes lesion size, reduces scarring, and preserves neuron survival after SCI. (**A**) Immunofluorescence staining of GFAP (green) and PDGFRβ (red) in sagittal sections from the CX3CL1 + M-CSF, CX3CL1, M-CSF and PBS groups at 28 dpi. ROI represents the high-magnification image within the dotted box on the left. Asterisks show the injured core. (**B** and **C**) Quantification of the percentage of $GFAP^{-}$ area (**B**) and $PDGFR\beta^{+}$ area (**C**) within the spinal cord segment spanning the injured core at 28 dpi ($n = 4$ mice per group). (**D**) Representative immunofluorescence images of $NeuN^{+}$ neurons in Z1–Z3 zones adjacent to central lesion core in the CX3CL1 + M-CSF, CX3CL1, M-CSF and PBS groups at 28 dpi. (**E**) Quantification of $NeuN^{+}$ neurons in Z1–Z3 zones adjacent to central lesion core in the CX3CL1 + M-CSF, CX3CL1, M-CSF and PBS groups at 28 dpi ($n = 3$ mice per group). The data are presented as means ± SEM (error bars). $^{*}P < 0.05$, $^{**}P < 0.01$, $^{***}P < 0.001$ and $^{****}P < 0.0001$, the CX3CL1 + M-CSF group versus the CX3CL1, M-CSF and PBS groups. Statistical analysis was performed using either one-way (**B** and **C**) or two-way (**E**) ANOVA followed by Bonferroni post hoc tests'. Scale bars = 200 μm (**A** and **D**), 20 μm (**ROI**).

Discussion

The present study elucidates a novel facet of adult microglial function in the healing dynamics of SCI. We propose that the advantageous roles of adult microglia are critically restricted by their post-injury spatial positioning, which is closely related to the reduction of the chemokine CX3CL1 and its perilesional distribution, as well as the dominant infiltration by macrophages. Our findings demonstrate that the co-administration of CX3CL1 and M-CSF significantly enhances both centripetal migration and prolonged retention of microglia, more effectively than either compound alone, thereby displacing macrophage infiltration and facilitating tissue repair. These results highlight the criticality of microglial location and abundance in the orchestration of SCI repair. In addition, we identify a potential link between the combined effects of CX3CL1 and M-CSF and the upregulation of SYK, a kinase that augments the phagocytic capacity of the centripetal microglia after SCI, offering novel insights into the targeted modulation of microglial functional activity.

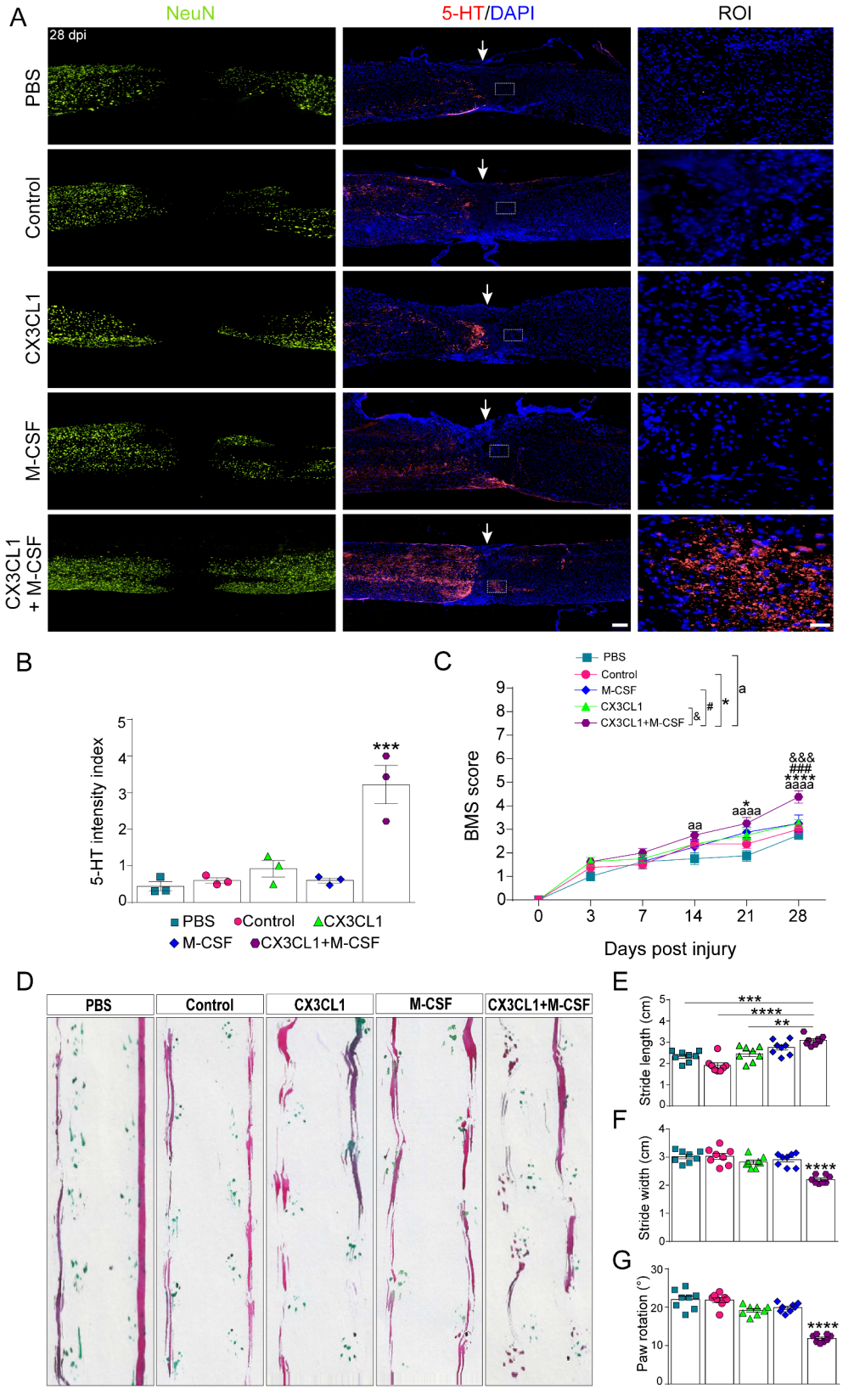

Fig. 6 (See legend on next page.)

(See figure on previous page.)

Fig. 6 Co-administration of CX3CL1 and M-CSF enhances axonal preservation/regrowth and improves locomotor function recovery after SCI. (**A**) Immunofluorescence staining of NeuN (green), 5-HT (red) and DAPI (blue) in sagittal sections from the CX3CL1 + M-CSF, CX3CL1, M-CSF, Control and PBS groups at 28 dpi. ROI represents the high-magnification image within the dotted box on the left. White arrowheads indicate the lesion site. (**B**) Quantification of 5-HT density within the spinal cord segment spanning the injured core of the CX3CL1 + M-CSF, CX3CL1, M-CSF, Control and PBS groups at 28 dpi ($n = 3$ mice per group). (**C**) Time course of functional recovery assessed by the BMS score after SCI ($n = 8$ mice per group). (**D**) Footprint analysis performed at 28 dpi reveals improved functional recovery in the CX3CL1 + M-CSF group ($n = 8$ mice per group). (**E**-**G**) Quantification of the footprint analysis parameters (stride length, stride width, and paw rotation) after SCI ($n = 8$ mice per group). The data are presented as means ± SEM (error bars). $^{aa}P < 0.01$ and $^{aaaa}P < 0.0001$, the CX3CL1 + M-CSF group versus the PBS group; $^{*}P < 0.05$, $^{**}P < 0.01$, $^{***}P < 0.001$, $^{****}P < 0.0001$, the CX3CL1 + M-CSF group versus the CX3CL1, M-CSF, Control and PBS groups; $^{\#\#\#}P < 0.001$, the CX3CL1 + M-CSF group versus the M-CSF group; $^{\&\&\&}P < 0.001$, the CX3CL1 + M-CSF group versus the CX3CL1 group. Statistical analysis was performed using either one-way (**B**, **E**-**G**) or two-way (**C**) ANOVA followed by Bonferroni post hoc tests. Scale bars = 200 μm (**A**), 50 μm (**ROI**).

Microglia are double-edged swords in the aftermath of SCI. While traditionally perceived as detrimental to recovery due to their release of pro-inflammatory cytokines and resultant neurotoxicity [28–31], emerging evidence supports a more nuanced role. Depletion of microglia disrupts glial scar formation, diminishes neuronal survival, exacerbates axonal dieback, and impairs locomotor recovery, thereby underscoring their beneficial contributions [2, 3]. The application of single-cell sequencing technology has significantly advanced our understanding of microglia, offering a deeper insight into cell subtypes associated with distinct functional properties [2, 32, 33]. Despite variations in classification, recent delineations categorize pre- and post-SCI microglia into several subtypes, each exhibiting unique temporal profiles and functional signatures. For instance, homeostatic microglia predominate in healthy conditions, while activated microglia emerge at 1–3 dpi, followed by proliferating microglia mostly observed at 3–7 dpi, phagocytosing microglia at 7 dpi, lipid processing microglia at 7–28 dpi, and patrolling microglia mainly evident at 28 dpi [2, 33–35]. These studies have illuminated temporal shifts in microglial functions and subtypes post-SCI, yet the impact of microglial location and distribution on their functionality and activity remains underexplored.

The disruption of the blood-spinal cord barrier (BSCB) post-SCI leads to the preferential infiltration of blood-derived macrophages into the injury core, culminating in the formation of foamy macrophages that aggravate inflammation and impede reparative processes [7, 36]. Kobayakawa et al. have confirmed that accelerating the C5a-directed centripetal migration of macrophages and curtailing their dissemination can significantly ameliorate tissue pathology and improve functional recovery after SCI [37]. Greenhalgh et al. shows that infiltrating macrophages may inhibit microglial phagocytic activity via the prostaglandin E2 (PGE2)/EP2 receptor signaling pathway [38]. These studies suggest that the perilesional distribution of microglia is related to the preferential site occupation of macrophages and their inhibitory influence on microglial function. Accordingly, we emphasize that altering microglial localization emerges as a valuable strategy, given their location-dependent functional effects.

The CX3CL1/CX3CR1 axis is implicated in microglial migration and their consequential role in SCI repair. Our study corroborates prior observations of reduced CX3CL1 expression post-SCI [39], and extends the understanding by revealing the perilesional distribution of CX3CL1 originating from neurons and endothelial cells around the lesion site. This reduction and distribution of CX3CL1 are suggested as potential reasons for microglia positioning at the injury edge. Meanwhile, we demonstrate that in-situ CX3CL1 injection can effectively and specifically promote centripetal microglial migration to supplant macrophage infiltration. In a study by Freria et al., the use of a $CX3CR1^{-/-}$ mouse model revealed that the deletion of CX3CR1 reporter promotes neuroprotection and augments plasticity in spared fibers after SCI, proposing a detrimental role for the CX3CL1/CX3CR1 axis in SCI [40]. However, contrasting results emerge from other studies in traumatic brain injury and SCI, where using a $CX3CR1^{-/-}$ mouse model confirms a beneficial function of this axis in microglia, assisting in neuronal preservation and promoting motor recovery [41, 42]. Here, our data indicate that CX3CL1 and M-CSF co-administration shows beneficial effects in WT and $CX3CR1^{+/-}$ mice, but these effects are specifically blocked in $CX3CR1^{-/-}$ mice.

Importantly, the co-administration of CX3CL1 and M-CSF has proved a superior strategy to promote the centripetal migration and prolonged retention of microglia, successfully supplanting blood-derived macrophages and optimizing wound healing and axonal preservation/regrowth more effectively than the individual administration of either molecule post-SCI. Despite the fact that CX3CL1 alone induces microglial centripetal migration, these microglia in the injured core undergo apoptosis and are significantly reduced at 28 dpi, thereby compromising their functionality. Conversely, M-CSF injection alone primarily promotes cell proliferation, yielding infiltrating macrophages in the lesion core. This underscores the significance of co-administering CX3CL1 and M-CSF to facilitate both centripetal migration and prolonged

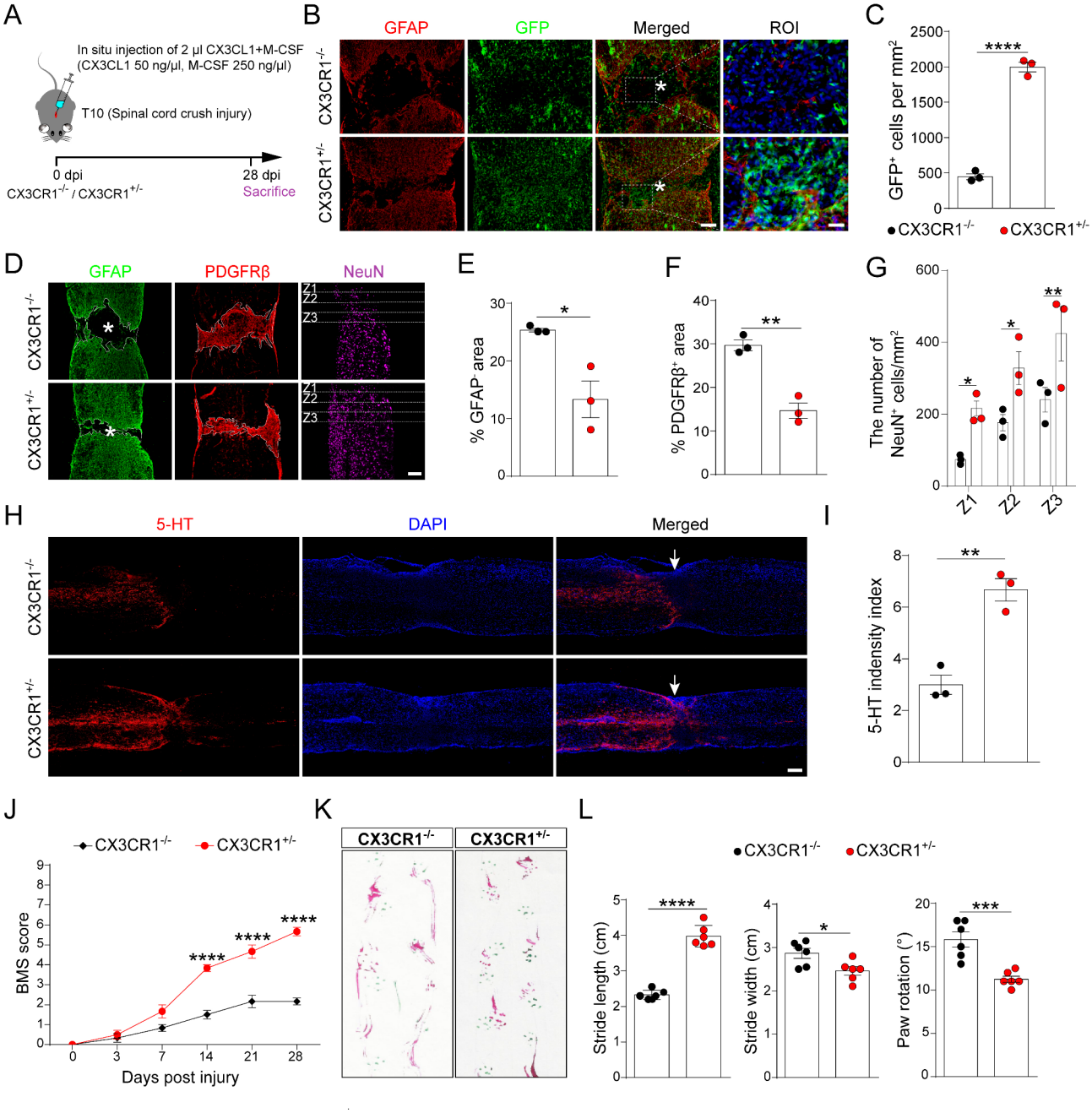

Fig. 7 (See legend on next page.)

(See figure on previous page.)

Fig. 7 The beneficial effects of combined administration of CX3CL1 and M-CSF are specifically blocked in CX3CR1$^{-/-}$ mice. **(A)** Schematic diagram illustrating in situ injection of 2 µl of CX3CL1 and M-CSF into the epicenter immediately after SCI in CX3CR1$^{-/-}$ (CX3CR1$^{GFP/GFP}$) and CX3CR1$^{+/-}$ (CX3CR1$^{+/GFP}$) mice. Histological analysis was performed at 28 dpi. **(B)** Representative immunofluorescence images of GFAP (red) and GFP (green) from sagittal sections of the injured spinal cord of CX3CR1$^{-/-}$ and CX3CR1$^{+/-}$ mice at 28 dpi. ROI represents the high-magnification image within the dotted box on the left. Asterisks show the injured core. **(C)** Quantification of the number of GFP^{+} microglia in the epicenter of CX3CR1$^{-/-}$ and CX3CR1$^{+/-}$ mice at 28 dpi ($n = 3$ mice per group). **(D)** Representative images of sections of the injured spinal cord of CX3CR1$^{-/-}$ and CX3CR1$^{+/-}$ mice at 28 dpi, stained with antibodies against GFAP (green), PDGFRβ (red) and NeuN (purple). **(E and F)** Quantification of the percentage of GFAP^{-} area (E) and PDGFRβ^{+} area (F) within the spinal cord segment spanning the injured core in CX3CR1$^{-/-}$ and CX3CR1$^{+/-}$ mice at 28 dpi ($n = 3$ mice per group). **(G)** Quantification of NeuN^{+} neurons in Z1–Z3 zones adjacent to central lesion core in CX3CR1$^{-/-}$ and CX3CR1$^{+/-}$ mice at 28 dpi ($n = 3$ mice per group). **(H)** Immunofluorescence staining of 5-HT (red) and DAPI (blue) in sagittal sections of the injured spinal cord from CX3CR1$^{-/-}$ and CX3CR1$^{+/-}$ mice at 28 dpi. White arrowheads indicate the lesion site. **(I)** Quantification of 5-HT density within the spinal cord segment spanning the injured core in CX3CR1$^{-/-}$ and CX3CR1$^{+/-}$ mice at 28 dpi. ($n = 3$ mice per group). **(J)** Time course of functional recovery of CXCR1$^{-/-}$ and CX3CR1$^{+/-}$ mice assessed by the BMS score after the combined treatment of CX3CL1 and M-CSF post-SCI ($n = 6$ mice per group). **(K)** Footprint analysis performed at 28 dpi reveals improved functional recovery in the CX3CR1$^{+/-}$ mice after the combined treatment of CX3CL1 and M-CSF. **(L)** Quantification of the footprint analysis parameters (stride length, stride width, and paw rotation) in CX3CR1$^{-/-}$ and CX3CR1$^{+/-}$ mice at 28 dpi ($n = 6$ mice per group). The data are presented as means ± SEM (error bars). $^{*}P < 0.05$, $^{**}P < 0.01$, $^{***}P < 0.001$ and $^{****}P < 0.0001$, the CX3CR1$^{+/-}$ mice versus the CX3CR1$^{-/-}$ mice. Statistical analysis was performed using two-way ANOVA (G and J) followed by Bonferroni post hoc tests', or Student's two-tailed unpaired t-test (**C**, **E**, **F**, **I** and **L**). Scale bars = 200 µm (**D** and **H**), 100 µm (**B**), 20 µm (**ROI**)

retention of microglia, which are crucial for tissue repair following SCI. We postulate that this co-administration fosters a beneficial microglial response through several mechanisms: (1) effective migration displacing macrophages and alleviating their inhibitory effect on microglial function; (2) sufficient microglial density and retention for reparative action; (3) the necessity of the CX3CR1 receptor engagement; (4) the association with heightened SYK expression, further supporting reparative processes.

SCI leads to neuronal and myelin debris accumulation, posing a formidable barrier to axonal regeneration and functional recovery [43]. The microglial clearance of such debris is critical in mitigating secondary neuronal damage [44]. SYK, known for its role in antifungal immune responses [45], has been implicated in microglial phagocytosis and neuroprotection in demyelinating diseases [26]. Our results suggest that the SYK upregulation in the centripetal microglia may be instrumental in the reduction of foamy macrophages, thus promoting functional recovery after SCI. Furthermore, our results posit that centripetal microglia exhibit stronger phagocytic and lipid metabolic capabilities compared to blood-derived macrophages, possibly due to the pronounced upregulation of SYK signaling. In addition, we observed that co-administration-induced SYK upregulation was suppressed in CX3CR1$^{-/-}$ mice, suggesting direct regulation of SYK activity in SCI by the CX3CL1/CX3CR1 axis.

There are several limitations that should be acknowledged. First, although young female mouse models provide methodological consistency, their clinical relevance may be limited given that 68.3% of traumatic SCI patients are male with a median age of 59.2 years [46]. While our study achieved adequate statistical power ($p < 0.05$, 95% CI), further validation through large-scale preclinical studies across diverse age groups and both sexes is necessary to confirm the biological relevance of these findings. Second, regarding methodological considerations, while Fascin-1 has proven valuable for microglial identification in SCI models [25], Cx3cr1^{CreERT2}::R26-tdTomato and Tmem119^{CreERT2}:: R26-tdTomato mice should enable more precise microglial tracking in future experiments. Third, the observed increase in 5-HT^{+} axon following treatment may be attributed to either neuroprotective effects or axonal regrowth, including regeneration and sprouting [47]. The specific underlying mechanisms require further investigation. Finally, the role of SYK in regulating microglia to promote their repair functions, and its potential as a therapeutic target for SCI, remains to be verified.

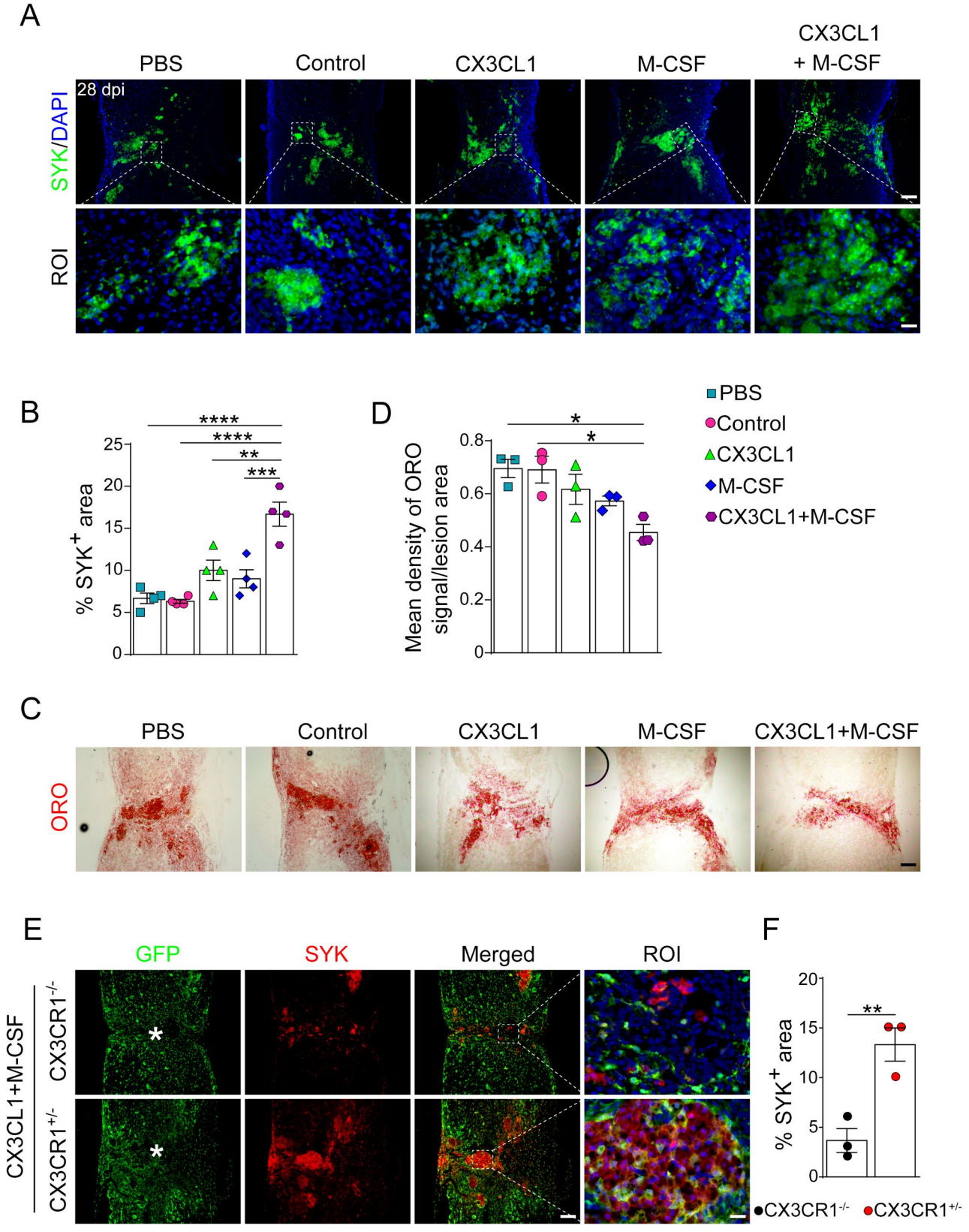

Fig. 8 (See legend on next page.)

(See figure on previous page.)

Fig. 8 Co-administration of CX3CL1 and M-CSF may exert beneficial effects by enhancing SYK levels in CX3CR1^{+} microglia and reducing foamy cell recruitment after SCI. (**A**) Immunofluorescence staining of SYK (green) and DAPI (blue) in sagittal sections from the CX3CL1 + M-CSF, CX3CL1, M-CSF, Control and PBS groups at 28 dpi. ROI represents the high-magnification image within the dotted box on the left. Asterisks show the injured core. (**B**) Quantification of the percentage of SYK^{+} area within the spinal cord segment spanning the injured core at 28 dpi ($n = 4$ mice per group). (**C**) Lipid accumulation was determined by ORO staining at 28 dpi. (**D**) The quantification of the ratio of the mean density of ORO signal to the lesion area within the spinal cord segment spanning the injured core at 28 dpi ($n = 3$ mice per group). (**E**) Representative immunofluorescence images of SYK (red) and GFP (green) in sagittal sections of the injured spinal cord from CX3CR1$^{-/-}$ and CX3CR1$^{+/-}$ mice at 28 dpi. These mice were treated with an in situ injection of 2 µl of CX3CL1 and M-CSF into the epicenter immediately after SCI. (**F**) Quantification of the percentage of SYK^{+} area within the spinal cord segment spanning the injured core in CX3CR1$^{-/-}$ and CX3CR1$^{+/-}$ mice at 28 dpi ($n = 3$). The data are presented as means ± SEM (error bars). $^{*}P < 0.05$ and $^{**}P < 0.01$, $^{***}P < 0.001$ and $^{****}P < 0.0001$. Statistical analysis was performed using one-way ANOVA followed by Bonferroni post hoc tests (**B** and **D**), or Student's two-tailed unpaired t-test (**F**). Scale bars = 200 µm (**A**, **C** and **E**), 20 µm (**ROI**)

Conclusions

In conclusion, our study establishes that the co-administration of CX3CL1 and M-CSF represents a superior strategy for promoting centripetal migration and prolonged retention of microglia after SCI. This combined intervention, targeting microglial reposition, effectively substitutes for blood-derived macrophages, thereby optimizing wound healing and facilitating axonal preservation/regrowth. These discoveries identify centripetal microglial dynamics as promising targets for SCI therapy.

Abbreviations

SCI	Spinal Cord Injury
CX3CL1	C-X3-C motif Chemokine Ligand 1
M- CSF	Macrophage colony-stimulating factor
CX3CR1	C-X3-C motif Chemokine Receptor 1
SYK	Spleen Tyrosine Kinase
CSF1R	Colony-Stimulating Factor Receptor
SPF	Specific Pathogen-Free
5- HT	5-Hydroxytryptamine
ORO	Oil Red O
TUNEL	Terminal deoxynucleotidyl transferase dUTP nick-end labeling
BMS	Basso Mouse Scale
SEM	Standard Error of the Mean
ANOVA	Analysis of variance
dpi	Days post-injury
ROI	Region of Interest
WT	Wild-Type
BSCB	Blood-Spinal Cord Barrier
PGE2	Prostaglandin E2

Supplementary Information

The online version contains supplementary material available at https://doi.org/10.1186/s12974-025-03411-9.

Supplementary Material 1

Supplementary Material 2

Supplementary Material 3

Acknowledgements

We are grateful for the support of the Scientific Research and Experimental Center of the Second Affiliated Hospital of Anhui Medical University.

Author contributions

Mg Z and Jh J designed and supervised the study. Jn Y and Fl S carried out the construction of mouse model and in situ injection. CL, Xz X and Ny Z performed the part experiments and data analysis with technical help from HH, Jj L, Fr Oy, Jw W, Yz Z, Cp M and Zd M. Zy L and Ss Y provided experimental guidance. Jn Y wrote the first draft of the manuscript, and all authors read, edited, and approved the final manuscript.

Funding

This study was funded by the National Natural Science Foundation of China (Grant Nos. 82372506 to Mg Z, 82401616 to Ss Y, 82301563 to Zy L), the Anhui Provincial Natural Science Foundation (Grant Nos. 2308085MH257 to Mg Z, 2208085MH222 to Jh J, 2308085QH266 to Zy L, 2408085QH262 to Ss Y); the Clinical Medical Research Transformation Project of Anhui Province (Grant Nos. 202304295107020014 to Mg Z, 202304295107020009 to Jh J); and the Natural Science Research Project of Anhui Educational Committee (Grant Nos. 2022AH050746 to Mg Z, 2022AH050713 to Zy L, KJ2021A0316 to Ss Y).

Data availability

No datasets were generated or analysed during the current study.

Declarations

Ethics approval and consent to participate

All procedures were carried out with the approval of the Ethics Committee of the Anhui Medical University (Approval No. LLSC20230809).

Consent for publication

Not applicable.

Competing interests

The authors declare no competing interests.

Author details

[1]Department of Orthopaedics, The Second Affiliated Hospital of Anhui Medical University, Hefei 230601, China
[2]Institute of Orthopaedics, Research Center for Translational Medicine, The Second Affiliated Hospital of Anhui Medical University, Hefei 230601, China

Received: 2 January 2025 / Accepted: 5 March 2025
Published online: 12 March 2025

References

1. Li Y, He X, Kawaguchi R, Zhang Y, Wang Q, Monavarfeshani A, et al. Microglia-organized scar-free spinal cord repair in neonatal mice. Nature. 2020;587:613–8.
2. Brennan FH, Li Y, Wang C, Ma A, Guo Q, Li Y, et al. Microglia coordinate cellular interactions during spinal cord repair in mice. Nat Commun. 2022;13:4096.
3. Bellver-Landete V, Bretheau F, Mailhot B, Vallières N, Lessard M, Janelle M, et al. Microglia are an essential component of the neuroprotective Scar that forms after spinal cord injury. Nat Commun. 2019;10:518.
4. Brennan FH, Swarts EA, Kigerl KA, Mifflin KA, Guan Z, Noble BT, et al. Microglia promote maladaptive plasticity in autonomic circuitry after spinal cord injury in mice. Sci Transl Med. 2024;16:eadi3259.
5. Zhu Y, Soderblom C, Krishnan V, Ashbaugh J, Bethea JR, Lee JK. Hematogenous macrophage depletion reduces the fibrotic Scar and increases axonal growth after spinal cord injury. Neurobiol Dis. 2015;74:114–25.
6. Milich LM, Ryan CB, Lee JK. The origin, fate, and contribution of macrophages to spinal cord injury pathology. Acta Neuropathol. 2019;137:785–97.
7. Wang X, Cao K, Sun X, Chen Y, Duan Z, Sun L, et al. Macrophages in spinal cord injury: phenotypic and functional change from exposure to Myelin debris. Glia. 2015;63:635–51.

8. Briones TL, Woods J, Wadowska M. Chronic neuroinflammation and cognitive impairment following transient global cerebral ischemia: role of fractalkine/cx3cr1 signaling. J Neuroinflammation. 2014;11:13.
9. Cook DN, Chen SC, Sullivan LM, Manfra DJ, Wiekowski MT, Prosser DM, et al. Generation and analysis of mice lacking the chemokine fractalkine. Mol Cell Biol. 2001;21:3159–65.
10. Poniatowski LA, Wojdasiewicz P, Krawczyk M, Szukiewicz D, Gasik R, Kubaszewski L, Kurkowska-Jastrzebska I, et al. Analysis of the role of cx3cl1 (fractalkine) and its receptor cx3cr1 in traumatic brain and spinal cord injury: insight into recent advances in actions of neurochemokine agents. Mol Neurobiol. 2017;54:2167–88.
11. Cardona AE, Pioro EP, Sasse ME, Kostenko V, Cardona SM, Dijkstra IM, et al. Control of microglial neurotoxicity by the fractalkine receptor. Nat Neurosci. 2006;9:917–24.
12. Jung S, Aliberti J, Graemmel P, Sunshine MJ, Kreutzberg GW, Sher A, et al. Littman DR. Analysis of fractalkine receptor cx(3)cr1 function by targeted deletion and green fluorescent protein reporter gene insertion. Mol Cell Biol. 2000;20:4106–14.
13. Hickman SE, Allison EK, Coleman U, Kingery-Gallagher ND, El KJ. Heterozygous cx3cr1 deficiency in microglia restores neuronal beta-amyloid clearance pathways and slows progression of Alzheimer's like-disease in ps1-app mice. Front Immunol. 2019;10:2780.
14. Ginhoux F, Greter M, Leboeuf M, Nandi S, See P, Gokhan S, et al. Fate mapping analysis reveals that adult microglia derive from primitive macrophages. Science. 2010;330:841–5.
15. Pons V, Laflamme N, Prefontaine P, Rivest S. Role of macrophage colony-stimulating factor receptor on the proliferation and survival of microglia following systemic nerve and cuprizone-induced injuries. Front Immunol. 2020;11:47.
16. Saederup N, Cardona AE, Croft K, Mizutani M, Cotleur AC, Tsou CL, et al. Correction: selective chemokine receptor usage by central nervous system myeloid cells in ccr2-red fluorescent protein knock-in mice. PLoS ONE. 2017;12:e176931.
17. Li Z, Zheng M, Yu S, Yao F, Luo Y, Liu Y, et al. M2 macrophages promote pdgfrbeta(+) pericytes migration after spinal cord injury in mice via Pdgfb/pdgfrbeta pathway. Front Pharmacol. 2021;12:670813.
18. Bhalala OG, Pan L, Sahni V, Mcguire TL, Gruner K, Tourtellotte WG, et al. Kessler JA. Microrna-21 regulates astrocytic response following spinal cord injury. J Neurosci. 2012;32:17935–47.
19. Streeter KA, Sunshine MD, Brant JO, Sandoval A, Maden M, Fuller DD. Molecular and histologic outcomes following spinal cord injury in spiny mice, acomys cahirinus. J Comp Neurol. 2020;528:1535–47.
20. Chen KS, Mcginley LM, Kashlan ON, Hayes JM, Bruno ES, Chang JS, et al. Targeted intraspinal injections to assess therapies in rodent models of neurological disorders. Nat Protoc. 2019;14:331–49.
21. Zhang Y, Zhao L, Wang X, Ma W, Lazere A, Qian HH, et al. Repopulating retinal microglia restore endogenous organization and function under cx3cl1-cx3cr1 regulation. Sci Adv. 2018;4:eaap8492.
22. Liu W, Ge X, Zhou Z, Jiang D, Rong Y, Wang J, et al. Deubiquitinase usp18 regulates reactive astrogliosis by stabilizing sox9. Glia. 2021;69:1782–98.
23. Wanner IB, Anderson MA, Song B, Levine J, Fernandez A, Gray-Thompson Z, et al. Glial Scar borders are formed by newly proliferated, elongated astrocytes that interact to corral inflammatory and fibrotic cells via stat3-dependent mechanisms after spinal cord injury. J Neurosci. 2013;33:12870–86.
24. Li Z, Yu S, Liu Y, Hu X, Li Y, Xiao Z, et al. Su16f inhibits fibrotic Scar formation and facilitates axon regeneration and locomotor function recovery after spinal cord injury by blocking the Pdgfrbeta pathway. J Neuroinflammation. 2022;19:95.
25. Yu S, Cheng L, Tian D, Li Z, Yao F, Luo Y, et al. Fascin-1 is highly expressed specifically in microglia after spinal cord injury and regulates microglial migration. Front Pharmacol. 2021;12:729524.
26. Ennerfelt H, Frost EL, Shapiro DA, Holliday C, Zengeler KE, Voithofer G, et al. Syk coordinates neuroprotective microglial responses in neurodegenerative disease. Cell. 2022;185:4135–52.
27. Wang S, Sudan R, Peng V, Zhou Y, Du S, Yuede CM, et al. Trem2 drives microglia response to amyloid-beta via syk-dependent and -independent pathways. Cell. 2022;185:4153–69.
28. Sun C, Deng J, Ma Y, Meng F, Cui X, Li M, et al. The dual role of microglia in neuropathic pain after spinal cord injury: detrimental and protective effects. Exp Neurol. 2023;370:114570.
29. Fan H, Tang HB, Shan LQ, Liu SC, Huang DG, Chen X, et al. Quercetin prevents necroptosis of oligodendrocytes by inhibiting macrophages/microglia polarization to m1 phenotype after spinal cord injury in rats. J Neuroinflammation. 2019;16:206.
30. Kroner A, Greenhalgh AD, Zarruk JG, Passos DSR, Gaestel M, David S. Tnf and increased intracellular iron alter macrophage polarization to a detrimental m1 phenotype in the injured spinal cord. Neuron. 2014;83:1098–116.
31. Tran AP, Warren PM, Silver J. The biology of regeneration failure and success after spinal cord injury. Physiol Rev. 2018;98:881–917.
32. Gong L, Gu Y, Han X, Luan C, Liu C, Wang X, et al. Spatiotemporal dynamics of the molecular expression pattern and intercellular interactions in the glial Scar response to spinal cord injury. Neurosci Bull. 2023;39:213–44.
33. Li C, Wu Z, Zhou L, Shao J, Hu X, Xu W, et al. Temporal and Spatial cellular and molecular pathological alterations with single-cell resolution in the adult spinal cord after injury. Signal Transduct Target Ther. 2022;7:65.
34. Milich LM, Choi JS, Ryan C, Cerqueira SR, Benavides S, Yahn SL, et al. Single-cell analysis of the cellular heterogeneity and interactions in the injured mouse spinal cord. J Exp Med. 2021;218:e20210040.
35. Hakim R, Zachariadis V, Sankavaram SR, Han J, Harris RA, Brundin L, et al. Spinal cord injury induces permanent reprogramming of microglia into a disease-associated state which contributes to functional recovery. J Neurosci. 2021;41:8441–59.
36. Guo L, Rolfe AJ, Wang X, Tai W, Cheng Z, Cao K, et al. Rescuing macrophage normal function in spinal cord injury with embryonic stem cell conditioned media. Mol Brain. 2016;9:48.
37. Kobayakawa K, Ohkawa Y, Yoshizaki S, Tamaru T, Saito T, Kijima K, et al. Macrophage centripetal migration drives spontaneous healing process after spinal cord injury. Sci Adv. 2019;5:eaav5086.
38. Greenhalgh AD, Zarruk JG, Healy LM, Baskar JS, Jhelum P, Salmon CK, et al. Peripherally derived macrophages modulate microglial function to reduce inflammation after Cns injury. Plos Biol. 2018;16:e2005264.
39. Donnelly DJ, Longbrake EE, Shawler TM, Kigerl KA, Lai W, Tovar CA, et al. Deficient cx3cr1 signaling promotes recovery after mouse spinal cord injury by limiting the recruitment and activation of ly6clo/inos + macrophages. J Neurosci. 2011;31:9910–22.
40. Freria CM, Hall JC, Wei P, Guan Z, Mctigue DM, Popovich PG. Deletion of the fractalkine receptor, cx3cr1, improves endogenous repair, axon sprouting, and synaptogenesis after spinal cord injury in mice. J Neurosci. 2017;37:3568–87.
41. Blomster LV, Brennan FH, Lao HW, Harle DW, Harvey AR, Ruitenberg MJ. Mobilisation of the Splenic monocyte reservoir and peripheral cx(3)cr1 deficiency adversely affects recovery from spinal cord injury. Exp Neurol. 2013;247:226–40.
42. Zanier ER, Marchesi F, Ortolano F, Perego C, Arabian M, Zoerle T, et al. Fractalkine receptor deficiency is associated with early protection but late worsening of outcome following brain trauma in mice. J Neurotrauma. 2016;33:1060–72.
43. Mar FM, Da ST, Morgado MM, Rodrigues LG, Rodrigues D, Pereira M, et al. Myelin lipids inhibit axon regeneration following spinal cord injury: a novel perspective for therapy. Mol Neurobiol. 2016;53:1052–64.
44. Wu YQ, Xiong J, He ZL, Yuan Y, Wang BN, Xu JY, et al. Metformin promotes microglial cells to facilitate Myelin debris clearance and accelerate nerve repairment after spinal cord injury. Acta Pharmacol Sin. 2022;43:1360–71.
45. Lionakis MS, Iliev ID, Hohl TM. Immunity against fungi. Jci Insight. 2017;2:e93156.
46. Barbiellini AC, Salmaso L, Bellio S, Saia M. Epidemiology of traumatic spinal cord injury: a large population-based study. Spinal Cord. 2022;60:812–9.
47. Zheng B, Tuszynski MH. Regulation of axonal regeneration after mammalian spinal cord injury. Nat Rev Mol Cell Biol. 2023;24:396–413.

Publisher's note